Noncontact Dipole Effects on Channel Permeation. VI. 5F- and 6F-Trp Gramicidin Channel Currents

Chad D. Cole,* Adam S. Frost,* Nephi Thompson,* Myriam Cotten,† Timothy A. Cross,† and David D. Busath*

*Center for Neuroscience and Department of Physiology and Developmental Biology, Brigham Young University, Provo, Utah 84062, and †Center for Interdisciplinary Magnetic Resonance at the National High Magnetic Field Laboratory, Institute of Molecular Biophysics and Department of Chemistry and Biochemistry, Florida State University, Tallahassee, Florida 32306 USA

ABSTRACT Fluorination of peptide side chains has been shown to perturb gramicidin channel conductance without significantly changing the average side chain structure, which, it is hoped, will allow detailed analysis of electrostatic modulation of current flow. Here we report a 1312-point potassium current-voltage-concentration data set for homodimeric channels formed from gramicidin A (gA) or any of eight fluorinated Trp analogs in both lecithin and monoglyceride bilayers. We fit the data with a three-barrier, two-site, two-ion (3B2S) kinetic model. The fluorination-induced changes in the rate constants were constrained by the same factor in both lipids. The rate constant changes were converted to transition-state free-energy differences for comparison with previous electrostatic potential energy differences based on an ab initio force field. The model allowed a reasonably good fit ($\chi_r^2 = 8.29$ with 1271 degrees of freedom). The measured changes were subtle. Nevertheless, the fitted energy perturbations agree well with electrostatic predictions for five of the eight peptides. For the other three analogs, the fitted changes suggested a reduced translocation barrier rather than the reduced exit barrier as predicted by electrostatics.

INTRODUCTION

Based on site-directed mutagenesis results (Imoto et al., 1988; Yool and Schwarz, 1991; Heinemann et al., 1992; Yang et al., 1993; Williamson and Sather, 1999), the permeabilities and selectivities of proteinaceous membrane channels often reflect charges on side chains projecting into the aqueous pore. In the case of gramicidin channels, the side chains project away from the channel lumen (Fig. 1), but polar side chains can still affect ion flow (Koeppe et al., 1990; Daumas et al., 1989, 1991; Becker et al., 1991; Fonseca et al., 1992; Andersen et al., 1998; Busath et al., 1998). This has also now been demonstrated in the potassium channel where side chains found to affect ion permeability in Shaker channels (Jan and Jan, 1990; MacKinnon and Yellen, 1990; Yool and Schwarz, 1991; Hartmann et al., 1991) are located just outside of the backbone-line selectivity filter in the KcsA channel crystal structure (Doyle et al., 1998). Consequently, through-space forces such as electrical dipole potentials from side chains must be sufficient to modulate channel currents under some conditions. It seems reasonable to explore how predictable and specific such potentials might be. Therefore, we have set out to determine the structural and functional effects of minor perturbations of the Trp side chain electrostatic potential produced by indole fluorination. This paper is the seventh in a series designed to explore the relationship between slight structural changes and conductance changes through molecular mechanics computations and kinetic modeling.

Eight gramicidin analogs were prepared using peptide synthesis by the introduction of an indole C5- or C6-fluorinated tryptophan at position 9, 11, 13, or 15. Cotten et al. (1999) showed by ab initio computations that fluorination at the indole C5 position increases the dipole moment of tryptophan by 90% and changes the orientation of the dipole relative to the current pathway by 8° (Fig. 2). Fluorination at the indole C6 position increases the dipole moment by 45% and changes the orientation by 35°. They also report, based on solid-state NMR measurements, that the fluorinated side chain structures for the 11-, 13-, and 15-mutants were minimally modified from the native structure. As a first approximation, therefore, we expect the change of the electric field in each of these different channels to depend primarily on the changes in the strength and orientation of the side chain dipole moment.

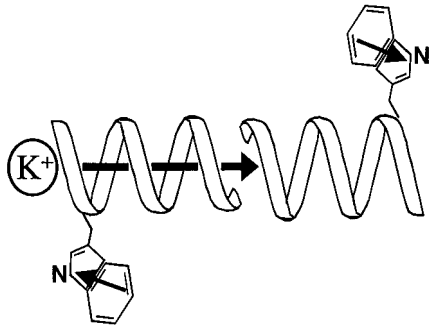

FIGURE 1 Schematic diagram of a gramicidin channel showing the location and orientation of a dimeric pair of tryptophan side chains and the orientation of the tryptophan dipole in relation to a permeating potassium ion.

Submitted February 20, 2002, and accepted for publication April 22, 2002.

C. D. Cole and A. S. Frost contributed equally to the project.

Address reprint requests to Dr. David D. Busath, Department of Physiology and Developmental Biology, Brigham Young University, Provo, UT 84602. Tel.: 801-378-8753; Fax: 801-378-7423; E-mail: david_busath@byu.edu.

0006-3495/02/10/1974/13 $2.00

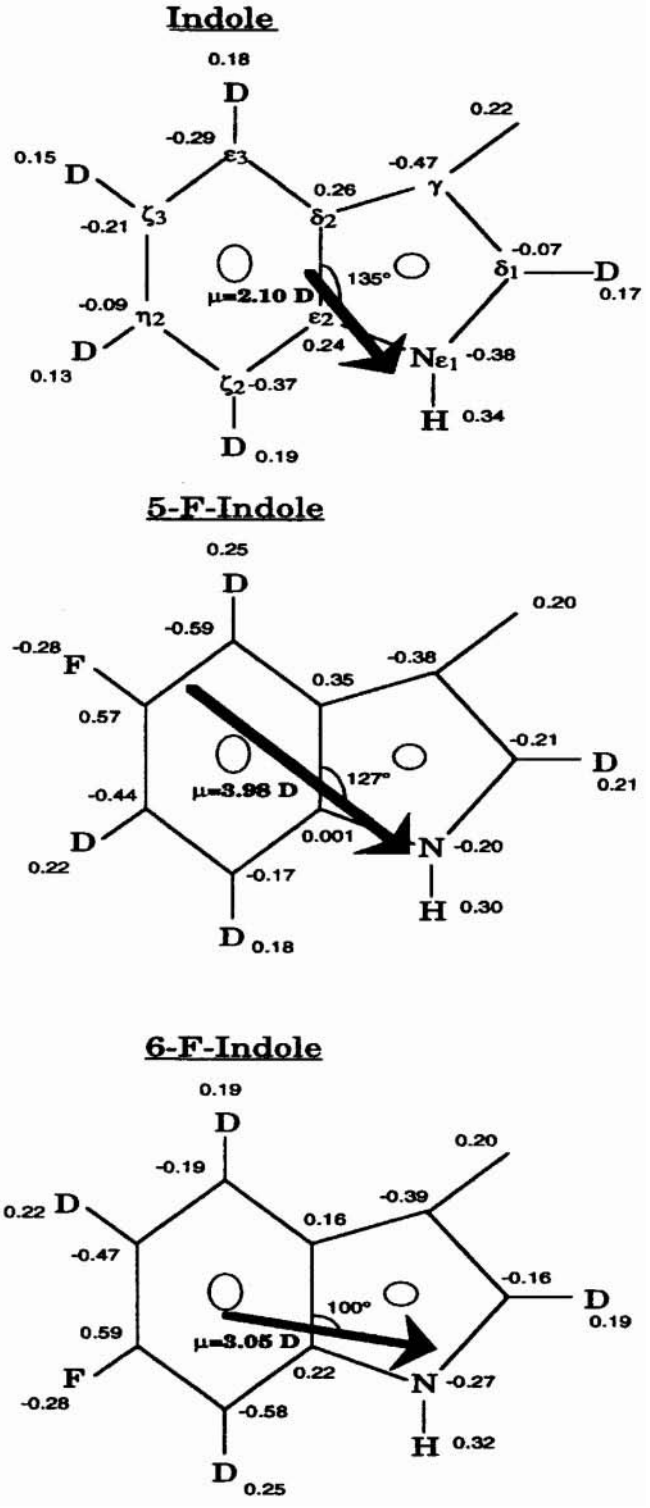

FIGURE 2 The ab initio partial charges computed by the electrostatic potential fitting method and the net dipole of native indole, 5F-indole, and 6F-indole as reported in Cotten et al. (1999).

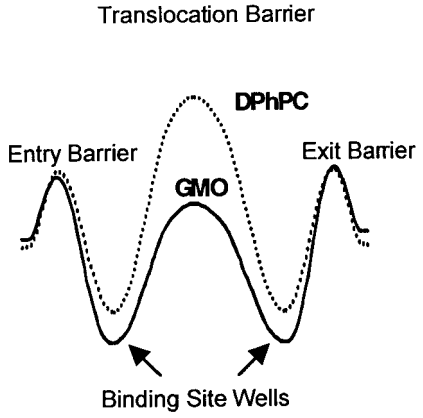

FIGURE 3 A stylized representation of the 3B2S free energy profile showing a higher translocation barrier for the DPhPC environment expected from interfacial dipole potential measurements (exaggerated for emphasis).

In previous studies, the Trp side chains have been shown to enhance gramicidin channel conductance, as demonstrated by a reduction of conductance upon replacement by nonpolar side chains (Heitz et al., 1986, 1988; Daumas et al., 1989; Becker et al., 1991). Trp 5-fluorination causes an enhancement in conductance in diphytanoyl phosphatidylcholine (DPhPC) bilayers (Andersen et al., 1998; Busath et al., 1998) and, for KCl at concentrations 2 M, an inhibition in glyceryl monoolein (GMO) bilayers (Busath et al., 1998). Although GMO is a nonphysiological monoglyceride, it is convenient to work with and provides a useful counterpoint to phosphocholine, helping to illuminate its high barrier to translocation. The barrier to translocation through the native gA channel appears to be considerably reduced in GMO compared with DPhPC because of a lower interfacial dipole potential (Pickar and Benz, 1978) (Fig. 3). Therefore, in GMO, entry or exit is likely to be the rate-limiting step and may be inhibited by the 5F-Trp dipole. This has been shown by current measurements with 5F-Trp$_{13}$ gA (Busath et al., 1998) using the 3B2S rate theory model in conjunction with coupling constants (Thompson et al., 2001). The coupling constants are used to reduce the number of free parameters in the model in a rational way. Here we make the same assumption concerning the interfacial dipole potential. Thus we assume that the perturbations are directly dependent on the partial charge structure in the fluorinated side chains and that the interfacial dipole potential contribution to the free energy profile is not affected by side chain fluorination.

Based on the ab initio partial charges for the side chains (Cotten et al., 1999), Anderson et al. (2001) recently computed the axial electrostatic potential energy of the side chains for native, 4F-, 5F-, and 6F-Trp in a gramicidin channel. The computations included corrections for water in the channel and bulk. The potentials were somewhat dependent on the sequence position of the Trp but could be summarized as follows (see Fig. 10 below for a complete display of the results). Each dimeric pair of native Trps (i.e., each pair of corresponding residues from the two mono-

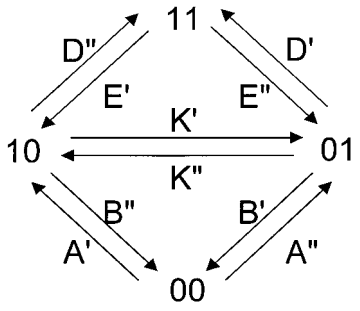

FIGURE 4 The four-state diagram for the 3B2S model of permeation. The left- and right-hand numbers for each state designate the occupancy of the two sites. The rate constants must be multiplied by voltage-dependency factors as specified in Urban and Hladky (1979). For the symmetric homodimer channels studied here and identical bathing solutions, the primed rate constants equal their unprimed counterparts.

mers) should stabilize an axial cation by ~ -0.6 kcal/mol throughout the channel. Replacement of a native pair with 5F-Trps should enhance stabilization at the center of the channel by an additional -0.4 to -0.6 kcal/mol with only minor effects on the energies at the entry and exit and therefore only minor effects on the entry and exit rate constants. In contrast, 6F-Trps should reduce the stabilization throughout the channel by approximately half, thereby enhancing the exit rate without affecting translocation rate. For the outermost Trp (6F-Trp_{15}), the reduction in stabilization at the center of the channel was not as great (only $\sim$0.1 kcal/mol), so translocation should also be enhanced.

The present study was performed to determine the single-channel currents for each of the fluorinated analogs. We focused on K^+ conductance because it was shown to be more responsive to fluorination effects than Na^+ in a previous study (Busath et al., 1998) and because K^+ is thought to follow a simpler reaction coordinate, remaining close to the axis of the channel (Kim et al., 1985). We then fit the data with the 3B2S rate theory model, constrained using the coupling technique developed by Thompson et al. (2001). We focused on the fluorination-induced changes in rate constants, which we compare to the changes in electrostatic energy computed by Anderson et al. (2001) under the logic that perturbations in the rate constants should reflect perturbations in the rates of the major steps according to the Boltzmann equation. It will be seen that this approach is successful for five of eight fluorinated analogs tested, but disagrees for three. Examination of the discrepancies leads to the suggestion that the outer 6F-Trps may interact with the interfacial waters, modifying their charge structure.

MATERIALS AND METHODS

Experimental procedures and equipment

Salt solutions were made with distilled water purified to >18 MΩ-cm with a Barnstead NANOpure II system (VWR Scientific, San Francisco, CA). Potassium chloride (Mallinckrodt, Paris, KY) was baked at >500°C for 1 h before use. Alkali metal concentration in solution was verified before use with a conductivity meter (Orion model 126). GMO (NuChek Prep, Elysian, MN), DPhPC (Avanti Polar Lipids, Birmingham, AL), *n*-hexadecane, and *n*-decane were used without additional purification.

Gramicidin A was purified from gramicidin D (ICN Pharmaceuticals, Cleveland, OH) by HPLC, and peptide solutions were prepared in MeOH and diluted to 10^{-5} mg/ml. (5F-indole)Trp and (6F-indole)Trp gramicidins were synthesized by solid-phase synthesis using Fmoc (9-fluorenylmethoxycarbonyl) chemistry on an Applied Biosystems (Foster City, CA) model 430A peptide synthesizer (Cotten et al., 1999). Isotopically labeled d4-indole 5-fluoro L-tryptophan and d4-indole 6-fluoro L-tryptophan were purchased from Cambridge Isotope Laboratories (Woburn, MA). Details of the synthesis and blocking chemistry have been described previously (Fields et al., 1989).

Lipid bilayers were formed as described previously (Busath et al., 1998). GMO was dispersed directly in hexadecane (50 mg/ml), and DPhPC in decane (20 mg/ml) was prepared from a DPhPC chloroform (10 mg/ml) solution. After the evaporation of chloroform, decane was added to the solid DPhPC and the solution was sonicated. Both lipid solutions were then painted with a polyethylene spatula under UV-free illumination on the aperture of a polyethylene pipette that had been inserted into a Teflon chamber and allowed to thin spontaneously. We then added 20- to 50-pg injections of gA or a 5F- or 6F-gA analog to the 2-ml chamber.

Membrane potentials were applied with Ag-AgCl electrodes. Membrane currents were measured using a List EPC7 patch-clamp amplifier (List Medical, Darsmstadt, Germany) or a Warner BC-525 bilayer clamp (Warner Instrument Corp., Hamden, CT). For each experiment, data were low-pass filtered with a cutoff frequency $f_c = 100$ Hz and collected continuously for up to 30 min after bilayer formation. Evaporative cooling and concentrating of the saline baths were minimized by efficient painting of bilayers and by placing a glass coverslip over the Teflon chamber. Data were collected on a Macintosh computer with a NI-DAQ data acquisition board (National Instruments, Austin, TX) and IGOR Pro Software (Version 3.01, Wave Metrics, Lake Oswego, OR). Current transitions reflecting channel openings and closings were detected and analyzed with TAC and TACfit software (Version 2.5, Skalar Instruments, Seattle, WA). Single-channel currents lasting less than $1/f_c$ were disregarded.

Statistical evaluation

In each experiment, the single-channel currents primarily fit within a normal distribution. Low-conductance (mini) channels did not vary in frequency or distribution for the different analogs and were generally ignored in the analysis. Likewise, single-channel noise and lifetimes were similar to those of native gA and were not evaluated in this study. Standard channel peak mean single-channel currents from at least three independent experiments were normalized to a 23°C room air temperature using $Q_{10} = 1.38$ and then averaged using the SD of the fitted normal curve as a weighting factor. If the SD among experiments was >0.1 pA the experiment was repeated. The uncertainty in applied membrane potential due to drift in the electrode potentials was <0.3 mV, and bath concentrations were prepared with an accuracy of 0.1%. Inter-experiment deviations were usually 2–3% of the conductance after temperature correction, probably because of discrepancies in the nominal bath concentration and temperature due to slight variations in evaporation. For *n* experiments with each analog, the uncertainty in the mean current (an average weighted by the SD of the standard channel peak) is computed from the inter-experiment SD(i) as:

$$\mathrm{SEM(i)} = \frac{\mathrm{SD(i)}}{\sqrt{n}} \tag{1}$$

These standard errors showed considerable variation because of the small sample size ($n = 3$ in most instances) but were correlated with the applied

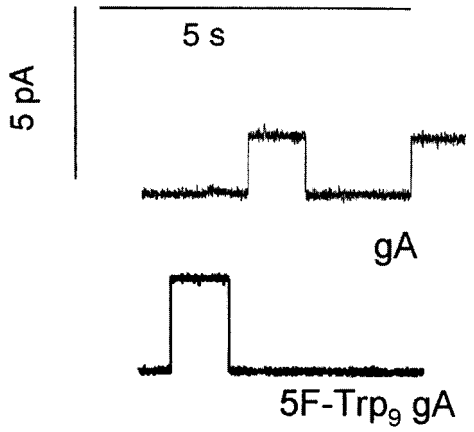

FIGURE 5 Single-channel current for gA and 5F-Trp$_9$ gA in DPhPC bilayers at 100 mV and 0.5 M KCl.

membrane potential, V_m. The weights used for fitting were therefore taken as the function representing the least-squares line through the SEM(i):

$$W_j = 0.0002(Vm_j) + 0.0116, \quad (2)$$

where the applied voltage for the jth point, Vm_j, is given in mV and W_j is in pA.

Model description

The 3B2S model was implemented using equations for the time derivatives of the occupancy state probabilities as described previously (Urban and Hladky, 1979; Thompson et al., 2001). The rate constants used in the model are given in Fig. 4, with A and D being concentration dependent.

The entry and exit rate constants depend exponentially on a fraction of the membrane potential defined by the electrical distances α_1 (the electrical (fractional) distance from the bulk solution to the peak of the entry barrier) and α_2 (the distance from the bulk solution to the minimum of the binding site). Because of the channel's twofold symmetry about the dimeric junction, the electrical locations of the exit-side binding site and exit barrier are 1-α_2 and 1-α_1, respectively, and the distance from bulk solution to the peak of the translocation barrier is 0.5. As a final refinement following the recommendation of Hladky (1999), a reduction of the voltage dependence of the translocation barrier was introduced as an additional parameter. This parameter, β (Urban et al., 1980; McBride, 1981), represents the electrical distance between two peaks separated by a shallow well (Hall et al., 1973) used to represent the central barrier and approximately represents the kind of trapezoidal barrier expected for an electrodiffusive process through a relatively flat chemical potential. Alternatively, the reduced voltage dependence of translocation could be interpreted as a net effect of orientation of the water by the ion in the pore and post-exit water reorientation (Roux and Karplus, 1993; Roux, 1999; Schumaker et al., 2001). The voltage dependencies of second ion entry and exit are set equal to those for first ion entry and exit to reduce excess freedom in the model.

TABLE 1 Conductance ratios relative to native gA

	DPhPC		GMO	
Lipid KCI (M)	0.1	2.0	0.1	2.0
5F-Trp$_9$	1.06	1.52	1.02	1.06
5F-Trp$_{11}$	1.10	1.48	0.92	1.11
5F-Trp$_{13}$	1.04	1.34	1.00	1.06
5F-Trp$_{15}$	1.00	1.45	0.80	1.10
6F-Trp$_9$	0.97	1.06	1.11	0.97
6F-Trp$_{11}$	0.98	1.21	1.06	0.96
6F-Trp$_{13}$	0.97	1.33	0.96	1.05
6F-Trp$_{15}$	0.95	1.31	1.02	1.08

Parameter coupling

We will refer to five rate constant parameters for gA in DPhPC bilayers and KCl solutions as our basis set. Rate constants for gA in GMO bilayers were coupled to the basis set parameters through coupling factors, which were included in the model as additional free parameters as explained in Thompson et al. (2001). Although this use of coupling parameters does not decrease the freedom of the model for describing these two data sets, on the grounds that the lipid environment energy differences would be the same for all peptides, we also used the same coupling parameters for each of the eight fluorinated analogs. We used the same three voltage-dependency parameters for all peptides, although we allowed them to differ according to lipid bilayer type. Therefore, the perturbations in rate constants due to side-chain potential changes were expected to be the same in both lipid bilayers and to have no effect on the locations of free energy extrema along the reaction coordinate. In addition, the changes in the free energies governing D and E (see Fig. 4), the rate constants for ion entry into a singly occupied pore and exit from a doubly occupied pore, were assumed to be the same as those governing A and B (Fig. 4), the first ion entry and exit rate constants, for all channel types. Thus, second ion rate constants were allowed to differ from first ion rate constants under the logic that ion-ion interactions would come into play, but these ion-ion interactions were assumed to be the same for all peptides.

To account for all nine channel types (gA and eight fluorinated analogs) with five rate constants and three voltage dependencies in two lipid types would require 144 separate parameters, but by coupling the parameters as described above we reduced the number of free parameters to only 40: the rate constants and voltage dependencies of the basis set (8), the changes in those parameters for the different bilayer type (8), and the changes in the single-ion rate constants A, B, and K for each of the fluorinated analogs (24). It should be noted that the 16 basis set parameters were quite similar to those obtained previously, especially those of Thompson et al. (2001). Therefore, the main supposition of our approach was that 20 current-voltage (I-V) relations for each peptide (10 bath concentrations for each of two lipids) would be enough to constrain three parameters for that peptide: the fluorination-induced change in entry, exit, and translocation rate constants.

Fitting algorithm and procedure

The data set of 1312 points was first fitted with 38 and later, adding β for the two lipids, with 40 free parameters using the Levenberg-Marquardt nonlinear least-squares algorithm. Goodness of the fit was determined using χ^2_r:

$$\chi^2_r = \frac{1}{\nu}\sum_j \frac{1}{W_j^2}[i_j - i(x_j)]^2, \quad (3)$$

where ν is the number of degrees of freedom (one less than the number of data points minus the number of free parameters); i_j is the jth data point; $i(x_j)$ the prediction of the function for the jth data point given all of the independent variables for that data point, x_j; and W_j is the uncertainty for the jth data point estimated from the linear fit to the SEM values shown above. Technically, an acceptable model ($p > 0.05$) requires that χ^2_r be less than ~2. However, we found fits with χ^2_r less than ~10 to be subjectively appealing.

Robustness of the fit was tested by variation of the parameter starting values. First, the parameters were assigned values from previously reported

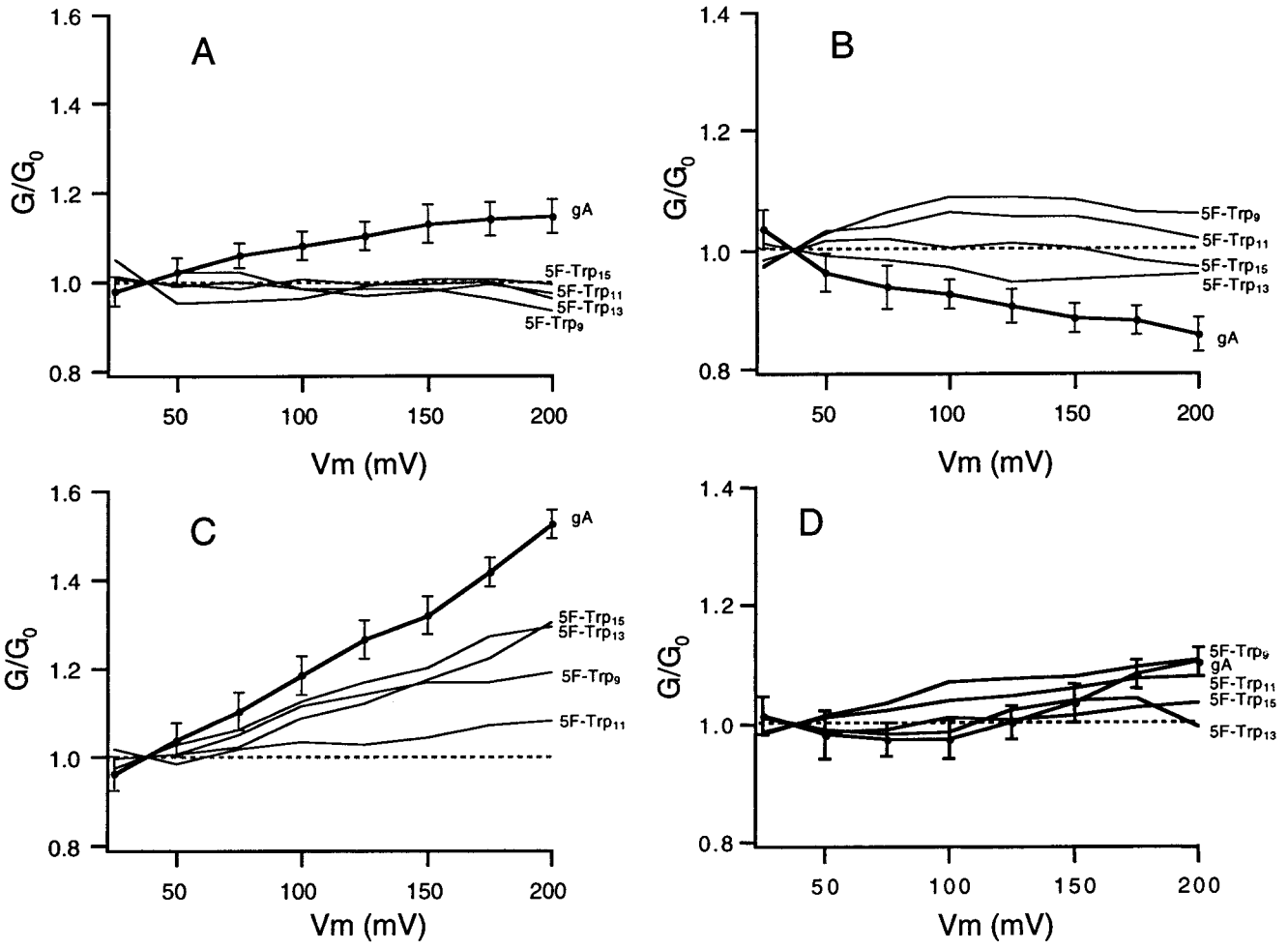

FIGURE 6 Normalized single-channel conductance versus membrane potential for gA and the 5F analogs. (*A* and *C*) Conductance in DPhPC bilayers; (*B* and *D*) Conductance in GMO bilayers; (*A* and *B*) 0.5 M KCl; (*C* and *D*) 2.0 M KCl. The normalization factor is the low-voltage conductance, the average of the conductances at 25 and 50 mV. Error bars (±SEM, computed by the method of propagation of errors), omitted for the analogs for clarity, are of similar amplitude to those shown for gA. Conductances were taken from standard-channel weighted-mean currents from three experiments, each normalized to 23°C.

kinetic models in the literature and allowed to vary until they reached a minimum. Second, the fluorination parameters were assigned to Anderson's predicted values and allowed to vary until they reached a minimum. We then constrained the basis set parameters and allowed the fluorination parameters to vary until they reached a minimum. This iterative process was repeated from several different starting points and with different degrees of constraint until the same parameter set was reached many different times. However, we found that there were many local minima in the vicinity of the best-fit parameters that the model could settle in. The only way to ensure that a given iteration would converge on the best fit was to start the first-ion well depth for the basis set (i.e., $-$RT ln A/B where A is at the standard [K^+], 1 M) within the interval of -2 to -3 kcal/mol, the regime expected from measured dissociation constants (Hinton et al., 1988; Wang et al., 1995).

To assess the sensitivity of the fit to variations in the underlying parameters, we computed χ^2_r contour maps by holding constant all but two parameters, which were varied on a grid. For this purpose, the rate constants were first converted to free energy parameters using the Eyring rate theory formulation (Hille and Schwarz, 1978).

The complete data set is available on the World Wide Web at http://bioag.byu.edu/zoology/gramicidin/index.html.

RESULTS

Single-channel currents for all eight analogs under all conditions studied were phenomenologically similar to those observed previously (Busath et al., 1998) with 5F-Trp_{13} gA. That is, single-channel lifetime, noise, and conductance dispersity were qualitatively unaffected. This is illustrated for 5F-Trp_9 gA in Fig. 5. This is especially important for the Trp_9 analogs, which were inaccessible to solid-state NMR studies (Cotten et al., 1999), and suggests that fluorination did not destabilize the side chain conformation in any way.

The effects of fluorination on channel conductance properties are illustrated by selected conductance ratios shown in Table 1 and normalized conductance-voltage plots shown

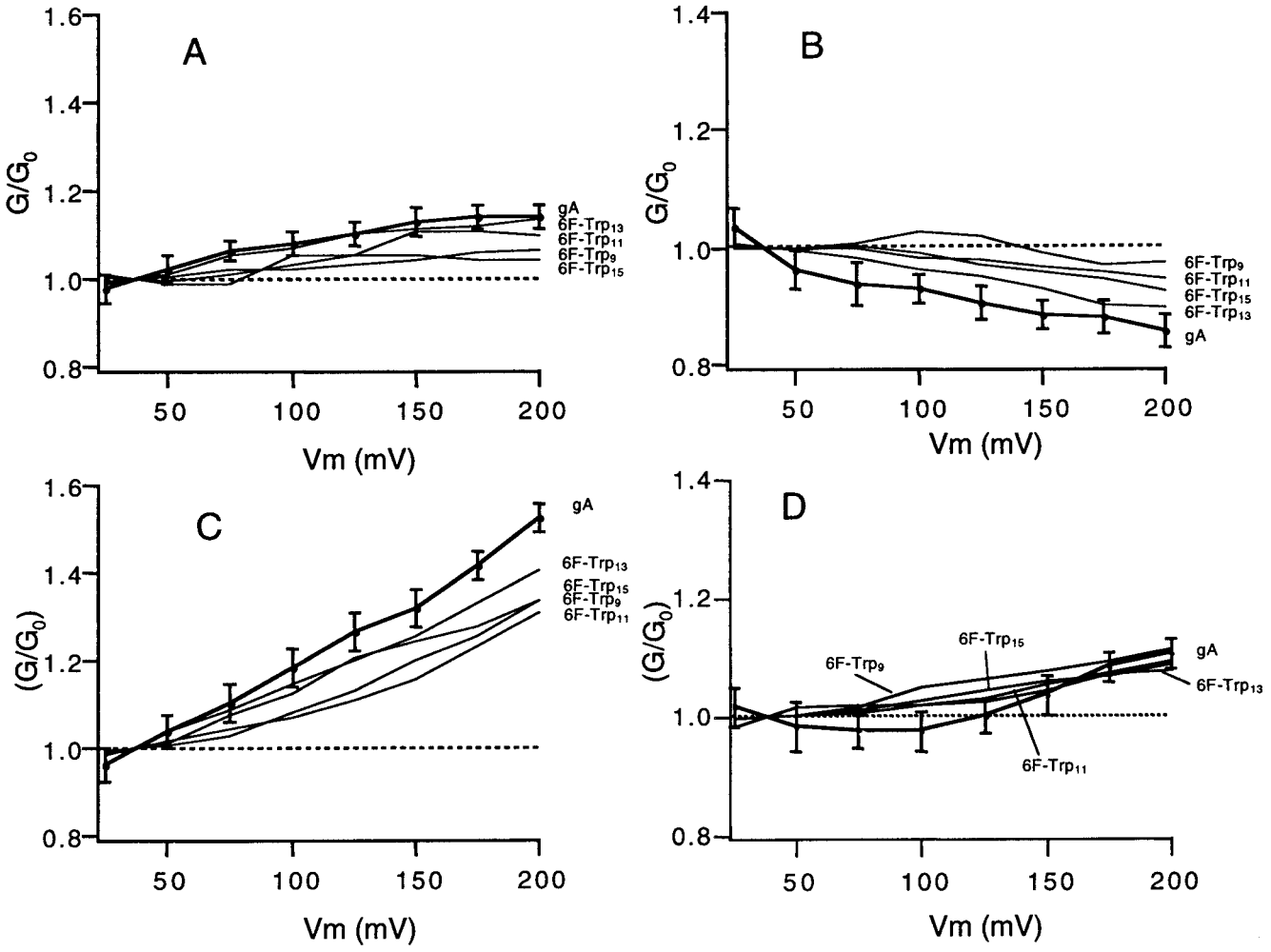

FIGURE 7 Identical to Fig. 5, but comparing the normalized conductance of gA with those of the 6F analogs.

for the 5F- and 6F-analogs in Figs. 6 and 7. The table gives the 50-mV conductance, relative to the gA 50-mV conductance, for the eight analogs in both lipids at low (0.1 M) and high (2.0 M) KCl. Figs. 6 and 7 demonstrate shifts in superlinearity due to fluorination for both lipids at moderate (0.5 M) and high (2.0 M) KCl. Table 1 shows that the changes in single-channel current because of fluorination were small but consistent. In DPhPC bilayers, all of the 5F-indole analogs of gA formed channels with larger single-channel currents than native gA in both high and low [KCl], reaching a maximum 52% increase in 2 M. The SE of the conductance ratio, relative to gA, for these measurements is <0.1 (Busath et al., 1998), so the uncertainty in the hypothesis that fluorination can enhance conductance is insignificant ($p < 0.05$). In GMO bilayers, the 5F-indole peptides had essentially the same single-channel currents as gA in 0.1 M KCl and a modest increase in conductance in 2.0 M KCl, averaging 8%. In DPhPC bilayers, all of the 6F-Trp analogs formed channels with smaller single-channel currents than gA in low [KCl] (3% average decrease) but exhibited larger currents than gA in high [KCl] (23% average increase). The single-channel currents of the 6F-Trp analogs in GMO bilayers did not reveal an obvious trend but were slightly increased or decreased depending on the position of the fluorinated tryptophan and the [KCl]. Overall, the change in the magnitude of the single-channel current was more noticeable in DPhPC bilayers than in GMO bilayers, and enhanced at higher [KCl].

Although the error bars in Figs. 6 and 7 are such that only in a few cases do analog conductances differ to a statistically significant level from each other or even gA, there are clear, reproducible trends in the means that display the effects of the modest perturbation when the measurements at all eight membrane potentials are examined. In DPhPC (left-hand panels), where fluorination clearly enhances conductance, both 5- and 6-fluorination are shown to reduce superlinearity (i.e., the normalized conductance does not exceed 1.0 as greatly), suggesting a decreased importance of voltage-dependent steps in limiting the rate of current flow. In energetic terms, this can be viewed as a decreased height

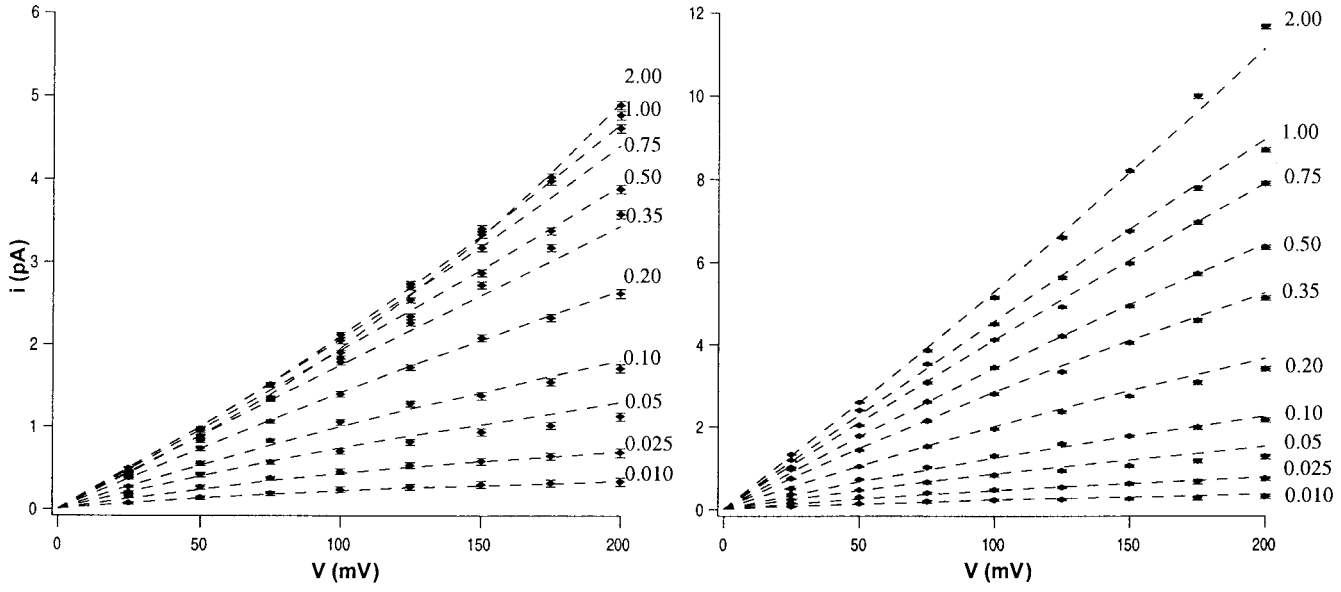

FIGURE 8 *I-V* plots of gA channels in 10 KCl concentrations with theoretical *I-V* values based on 3B2S parameters from Tables 2 and 3 plotted as dashed lines. DPhPC data are on the left and GMO data are on the right. Error bars are ±SEM.

of a highly voltage-dependent barrier, such as the translocation barrier (Busath et al., 1998; Thompson et al., 2001). This effect is greater for the 5F-analogs (Fig. 6, *A* and *C*) than for the 6F-analogs (Fig. 7, *A* and *C*) but is evident in both moderate (panels *A*) and high (panels *C*) concentrations. It may be significant in this regard that the gA conductance is superlinear at both concentrations. It has been proposed that the persistence of superlinearity at moderate concentrations in DPhPC probably reflects a large translocation barrier in this lipid because of interfacial dipole potential (Busath et al., 1998) and hence that fluorination is effective at enhancing conductance. In GMO bilayers, where fluorination has only minor effects on conductance (Table 1), the gA *I-V* is sublinear at moderate concentrations (panels *B*) and oscillates about linear at high concentrations (panels *D*). Under these conditions, fluorination mostly increases superlinearity (except at high membrane potentials in high concentrations as shown in panels *D*). Again, the effect, this time in the opposite direction, is somewhat greater for the 5F- than for the 6F-analogs. This effect is small but suggests that when the barrier to translocation is not significant, the remaining rate-limiting barrier is still voltage dependent and is increased by fluorination. One might expect the exit barrier to be a likely candidate as it is expected to be more rate limiting and voltage dependent than entry (Urban et al., 1980).

The *I-V* plots in Figs. 8 and 9 show the complete 1312-point data set, together with the best fit of the constrained 3B2S model (dashed lines). The parameters for the fit, which had $\chi^2_r = 8.29$, are given below in Tables 2–4. The *I-V* fits to the experimental data points for gA in DPhPC bilayers (Fig. 8, right panel) and in GMO bilayers (Fig. 8, left panel) and for the fluorinated analogs shown in Fig. 9 are qualitatively acceptable, although occasional discrepancies occur. The theoretical *I-V* values predict self-block (i.e., reduction in the conductance at high ion concentrations) in DPhPC bilayers, whereas in GMO bilayers the fit shows no self-block in agreement with the experimental data. However, in DPhPC bilayers the model predictions deviate at high [KCl]. In addition, the model overestimates the 6F-analog currents for both bilayer types at the lowest [KCl] and deviates in the intermediate [KCl] region (0.1–0.75 M), where the channel is thought, because of a change from sub- to superlinearity in the *I-V*, to transition from single to double occupancy. However, although there are some discrepancies in the fit, the gA parameters agree generally with several independent measurements, as will be discussed below, and can be taken as a reasonable first approximation of the transport kinetics.

Table 2 gives the basis set parameters for first ion entry, exit, and translocation (in DPhPC bilayers) in the first row and the coupling factor for the lipid or fluorinated peptide in the subsequent rows. The rate constant for entry into gA in GMO bilayers is A^{Basis} times the lipid coupling factor. The rate constant for entry into one of the fluorinated peptides in DPhPC is A^{Basis} times the analog coupling factor. For analogs in GMO, the lipid coupling factor is also included. The same approach was used with exit and translocation rate constants. Table 3 gives the basis parameters for second ion entry and exit. The lipid and analog coupling factors were the same as those used for first ion entry and exit in Table 2.

Table 2 indicates that 5-fluorination slightly decreases *A*, the rate of first ion entry (9% average decrease), negligibly decreases *B*, the rate of first ion exit (2% average decrease),

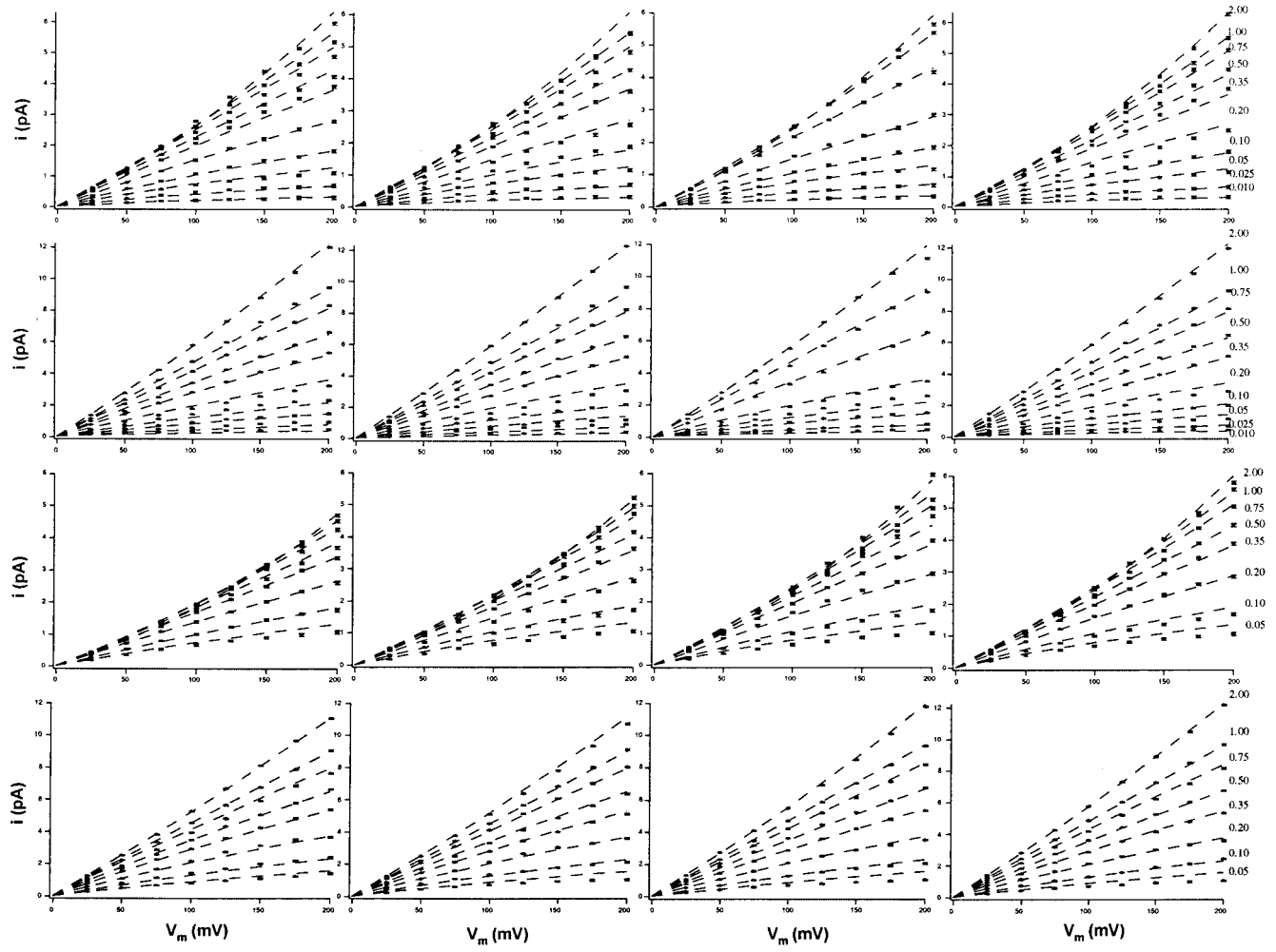

FIGURE 9 *I-V* plots of 5F- and 6F-analogs of gA channels in 8–10 KCl concentrations with theoretical *I-V* values based on 3B2S parameters plotted as dashed lines. The first two rows are *I-V* plots for the 5F-analogs, with the upper row showing *I-V* in DPhPC bilayers and the lower row showing *I-V* in GMO bilayers. The order of the peptides in terms of fluorinated Trp position, from left to right, is 9, 11, 13, and 15. The second two rows are *I-V* plots for the 6F-analogs, again with DPhPC data in the upper row and GMO data in the lower, and the same peptide order from left to right. Error bars are ±SEM, and the currents are normalized to 23°C.

and increases *K*, the rate of ion translocation (41% average increase). 6- Fluorination negligibly increases *A* (1% average increase), decreases *B*, (5% average decrease), and increases *K*, (18% average increase). From the lipid coupling parameter, it can also be seen that in GMO bilayers *A* is slightly increased (4%), *B* is significantly increased (133%), and *K* is greatly increased (876%). According to Table 3, *D*, the rate of second ion entry, is also increased by 4% in GMO whereas *E*, the rate of second ion exit, is reduced by 27%. Based on the size of the error bars in Figs. 6 and 7, and considering the robustness tests and sensitivity analysis to be described below, we consider differences of 10% or greater to be nonrandom and reliable.

Table 4 shows that the voltage dependency for the entry steps are nearly the same in DPhPC and GMO, 0.056 versus 0.065, respectively, as are the well positions, 0.24 and 0.30 for DPhPC and GMO, respectively. The well position for GMO is somewhat deeper than previously reported (Hladky and Haydon, 1984). However, this model includes a third voltage-dependency parameter, β, the electrostatic distance between the two peaks of a Hladky-style central barrier (Urban et al., 1980). It is interesting to note that in DPhPC bilayers, the distance between the double peaks is somewhat less than the distance between the two wells, 0.31 versus 0.52, indicating a more rounded barrier, whereas in GMO, β assumes the maximum width allowed (0.4, the distance between the two wells), suggesting a rectangular barrier with maximal voltage dependency. These may reflect differences between the two lipids in interfacial dipole potential.

TABLE 2 Basis first ion rate constants (DPhPC and gA) and coupling factors

	$A \times 10^8$ M^{-1} s^{-1}	$B \times 10^6$ s^{-1}	$K \times 10^7$ s^{-1}
Basis	1.70	3.07	1.43
Lipid	1.04	2.33	8.76
5FW9	0.93	0.93	1.53
5FW11	0.91	1.05	1.34
5FW13	0.94	0.94	1.35
5FW15	0.87	1.01	1.42
6FW9	1.02	1.03	0.87
6FW11	1.01	0.89	1.14
6FW13	1.01	0.91	1.34
6FW15	1.00	0.96	1.37

Fig. 10 displays the fluorination-induced perturbations of the parameters from the 3B2S fitting in comparison with the electrostatic predictions computed using CHARMM by Anderson et al. (2001). The bars show the fluorination-induced changes in barrier free energies taken from the coupling constants according to the following equations:

$$\Delta G_b = -RT \ln A_f/B_f \quad (4)$$

$$\Delta G_{cb} = -RT \ln K_f A_f/B_f \quad (5)$$

$$\Delta G_{tb} = \Delta G_{cb} - \Delta G_b = -RT \ln K_f \quad (6)$$

ΔG_b is the change in first ion binding affinity induced by fluorination, with negative values denoting tighter binding. ΔG_{cb} is the fluorination-induced change in the height of the central barrier (relative to the standard state, infinite separation of the ion from the channel), with negative values denoting a decrease in the barrier height. The relative translocation barrier change, ΔG_{tb}, is the difference between these two.

Overall, the fitted 3B2S parameters predict that the increase in single-channel current for both 5F- and 6F-indole analogs is due to a reduction in ΔG_{tb}. Comparison of the two right-hand bars for each of the eight peptide groupings shows that this result agrees with Anderson's electrostatic predictions, at least in sign. The only exception to this trend is for 6F-Trp_9, which (as shown in Table 1) has single-channel currents that are less distinguishable from gA single-channel currents. Both the 3B2S parameters and the electrostatic calculations agree that the relative translocation barrier is increased rather than decreased for 6F-Trp_9.

The agreement between the electrostatic predictions and the 3B2S parameters is especially good for the 5F-Trp analogs. For 5F-Trp_9 and 5F-Trp_{11} gA, the well depth is raised (see the first pair of bars) and the central barrier is decreased (see the middle pair of bars) for both approaches. For 5F-Trp_{13} and 5F-Trp_{15} gA, both the well and the central barrier are lowered, whereas the central barrier is lowered proportionately more, leading to a decrease in the relative translocation barrier.

TABLE 3 Basis second ion rate constants and coupling factors

	$D \times 10^8$ M^{-1} s^{-1}	$E \times 10^7$ s^{-1}
Basis	1.09	5.40
Lipid	1.06	0.73

TABLE 4 Electrical distance and central barrier voltage dependency

	Entry (A)	Site ($A + B$)	β (affects K)
DPhPC	0.056	0.24	0.31
GMO	0.065	0.30	0.40

For 6F-Trp_9, both models agree in that they predict an increase in the relative translocation barrier. However, the agreement between electrostatic predictions and 3B2S data-constrained parameters is poor for the 6-fluorinations at positions 11,13, and 15. Electrostatics predicted an increase in both the well and the central barrier, whereas the 3B2S parameters predict a decrease in both the well depth and the central barrier. Thus the net barrier for crossing the channel is predicted to decrease in both approaches, but the 3B2S fitting of the current data set indicate that it is a result of deepening the wells while lowering the central barrier even more, whereas the electrostatic prediction is that the wells become more shallow and the central barrier is also raised, but not as much.

Three alternative approaches to fitting the current data set were undertaken to examine the robustness of this discrepancy, As shown in Fig. 11, they all yielded similar results, reinforcing the disagreement between model parameters and electrostatic computations for 6F-Trp_{11}, 6F-Trp_{13}, and 6F-Trp_{15} gA. First, we calculated the sensitivity of our model to each of the five rate constants for the voltage and concentration ranges included in our data set (data not shown) and selected regions of the data that were most sensitive to (or rate limited by) one of the five rate constants The weights in the χ^2_r equation for the selected region of data were increased by 10-fold. The sensitivity analysis indicated that for changes in the depth of the binding site, currents in 0.05, 0.10, and 0.20 M KCl and from 150 to 200 mV should be more weighted. To focus on central barrier changes, currents in 0.35, 0.50, 0.75, 1.00, and 2.00 M KCl and from 75 to 125 mV should be weighted. To focus on entry barrier changes, currents in 0.01 and 0.025 M KCl and from 125 to 200 mV should be weighted. After several iterations of focused fitting, where only the parameters governing one of these three processes were free to change while the corresponding currents were weighted, the process converged to the parameter profile shown in the upper panel of Fig. 11.

The second panel in Fig. 11 displays the results of the same procedure explained above, but initializing the parameters to Anderson's predicted values rather than the parameters in Tables 2–4. The procedure represented by the third

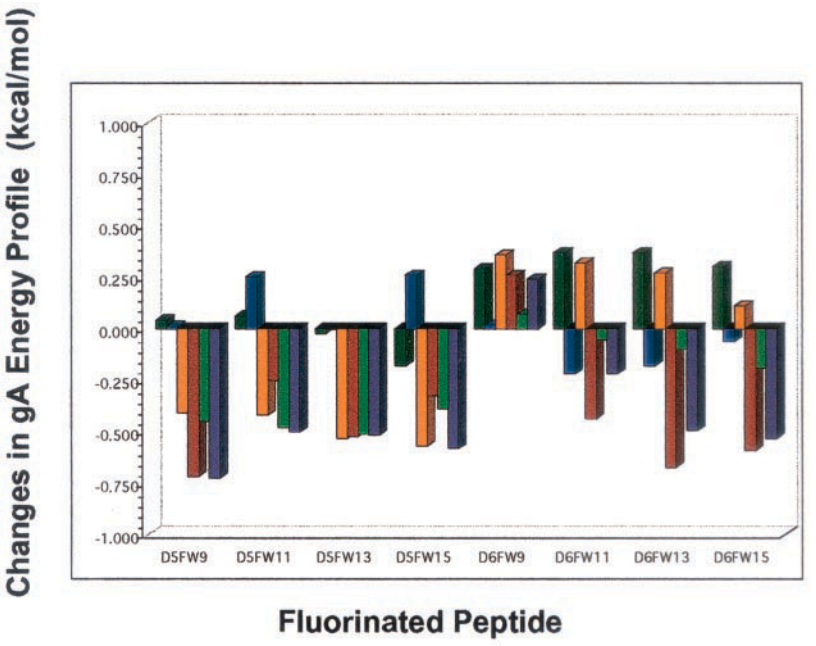

FIGURE 10 Comparison of electrostatic predictions (Anderson et al., 2001) and the 3B2S fitted parameters from Table 2 for the changes in the potential energy surface of the gramicidin barrier diagram for all eight fluorinated analogs. For each peptide, the bars show the change from the native gA value of the following (left to right): dark green, predicted well (depth relative to bath); blue, - fitted well depth (relative to bath); orange, predicted central barrier height (relative to bath); red, fitted central barrier height (relative to bath); green, predicted translocation barrier height (central barrier height minus well depth); purple, fitted translocation barrier height (central barrier height minus well depth).

panel differs from that shown in the first panel in that the parameters representing well depth and central barrier were allowed to vary together (20 free parameters at the same time, namely, two free rate constants for the native gA and each of the eight analog peptides and the two lipid dependency parameters). It is obvious that none of the changes increased the similarity to the electrostatic predictions.

Fig. 12 is a χ^2_r contour plot that indicates the sensitivity of the model to the height of the relative translocation barrier. Using the best-fit parameters from Tables 2–4, all of the parameters were constrained to be constant except the basis set values for *B* and *K*. These were varied so that the depth of the binding site well and the height of the central barrier were varied incrementally, and χ^2_r was recalculated at each grid point. The center of the plot corresponds to the minimum in χ^2_r, and the contour lines indicate a rising χ^2_r value. Consistent with the results for fluorination-induced perturbations in Figs. 10 and 11, the goodness of the overall fit is very sensitive to the relative translocation barrier, or the difference in energy between the binding site and the central barrier used in the basis set. There is a long valley in the contour surface where χ^2_r is relatively constant despite significant changes in the values of the binding site and central barrier energies, demonstrating the importance of the translocation rate constant to the goodness of the fit and emphasizing the inherent correlation between the translocation rate, *K*, and the exit rate, *B*. In careful comparisons of rounded, trapezoidal, and double-peaked translocation barriers following the methodology used previously to analyze silver anomalous mole fraction data (McBride, 1981), the double-peaked translocation barrier produced a somewhat better overall fit (data not shown) but did not modify the basic conclusions about the weakness in the three 6F-Trp fits nor the correlation between *K* and *B*.

DISCUSSION

C5-fluorination of gA tryptophan residues enhances conductance at high $[K^+]$ while reducing superlinearity in DPhPC bilayers and increasing superlinearity in GMO bilayers. At low $[K^+]$, the inhibition of conductance noted previously for 5F-Trp_{13} gA also occurs for 5F-Trp_{15} gA but is reversed for 5F-Trp_9 and 5F-Trp_{11} gA. These observations suggest that although fluorination reduces the translocation barrier, it also affects both the entry and exit barriers, depending on which residue is modified. The fitted 3B2S parameters indicate that 5-fluorination does reduce the central barrier and increase the entry barrier but that the effect on the exit barrier is negligible and varies with fluorinated Trp position.

Single-channel currents from gA channels C6-fluorinated at Trp positions 13 and 15 have increased conductance, decreased superlinearity, and decreased self-block in DPhPC. The same changes occur, but to a lesser extent, in GMO bilayers, except that superlinearity is increased. Opposite or no effects are generally observed for 6-fluorination at position 9. These results are consistent with electrostatic predictions (Anderson et al., 2001) and the 3B2S fitted parameters, indicating that the relative translocation barrier, the difference in energy between the depth of the binding site well and the peak of the central barrier, is reduced for all 6F analogs except 6F-Trp_9.

The basis set parameters obtained for the fit of K^+ currents in gA shown in Tables 2–4 are consistent with

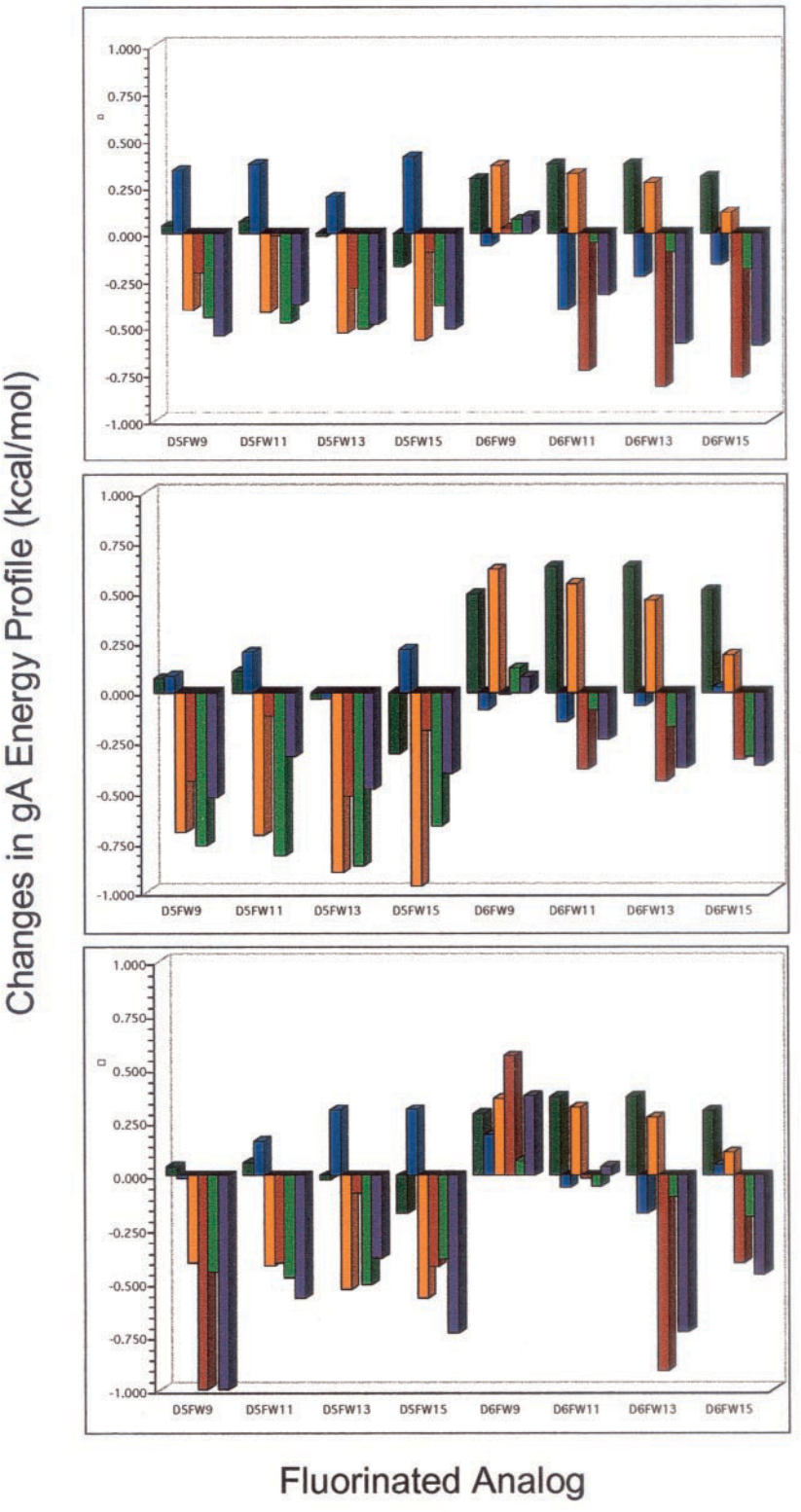

FIGURE 11 Comparison of electrostatic predictions and 3B2S parameters, using the same format as in Fig. 10 (including bar order and coloring), but for different fits (see text for details).

several independent measures. The 3B2S prediction of the first ion K^+ dissociation constant for gA in DPhPC bilayers agrees with Tl-205 NMR measurements of the equilibrium constant for K^+ with gA channels in lipid vesicles (Hinton et al., 1988). From an Arrhenius analysis, Tl-205 NMR yields a K^+ complex formation energy of $\Delta G = -2.4\% \pm 5\%$ kcal/mol, whereas the 3B2S basis parameters yield $-RT \ln B/A = -2.37$. The 3B2S model precisely estimates the rate of K^+ association with the channel based on current measurements at very high membrane potentials as well

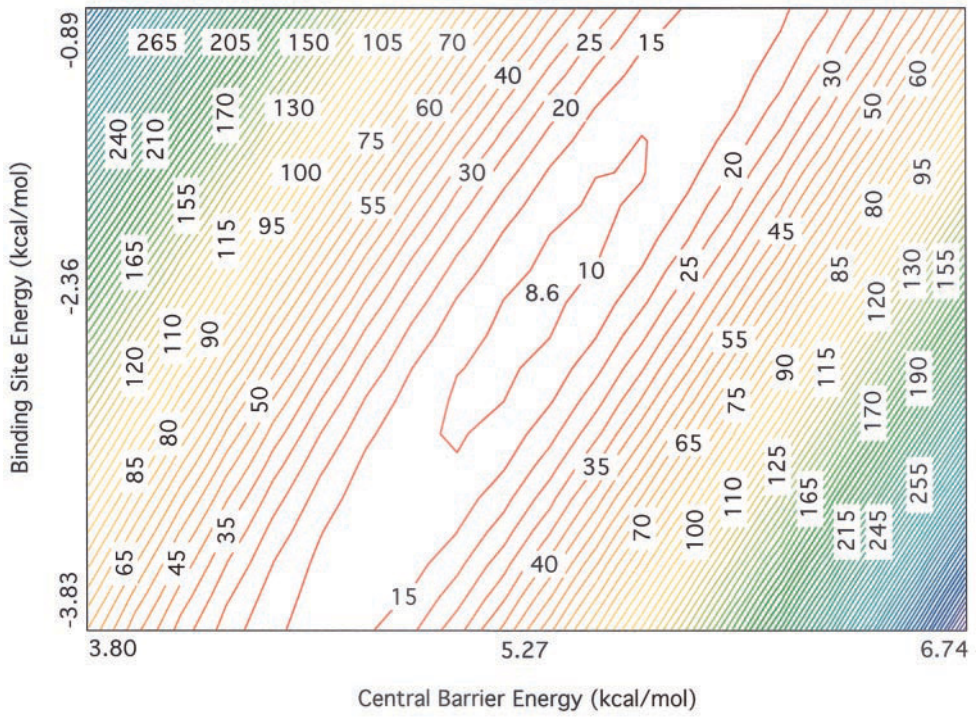

FIGURE 12 Contour plot showing the variation in χ^2_r for the 3B2S model using the parameters from Tables 2 and 3 with changes in the basis set parameters in terms of the depth of the binding site well and the height of the central barrier computed using the Boltzmann equation. The lowest point of the valley represents the best fit parameters ($\chi^2 = 8.29$).

(Andersen, 1983). In DPhPC, the maximal rate of entry for K^+ into the channel was found to be 1.7×10^8 ions M^{-1} s^{-1} and the corresponding 3B2S parameter in Table 2, A^{Basis}, is 1.70×10^8 ions M^{-1} s^{-1}. In GMO, the maximal rate of entry for K^+ into the channel is 1.9×10^8 ions M^{-1} s^{-1} and the 3B2S equivalent parameter, the lipid coupling parameter times A^{Basis}, is 1.77×10^8 ions M^{-1} s^{-1}.

The fluorination-induced energy perturbations obtained from the 3B2S fit here (Fig. 10) indicate that translocation is enhanced for 5F-Trp compounds with binding unaffected, as predicted by Anderson et al. (2001). For 6F-Trp_9 gA, binding is only slightly destabilized where Anderson et al. predict a large destabilization, but the increase in central barrier height is about the same in the two approaches. For the remainder of the 6F-analogs, the 3B2S fits yield energy perturbations more similar to those found for the 5F-analogs (i.e., decreased translocation barrier height), albeit with somewhat increased binding affinity. This finding was robust, as shown using three alternative fitting procedures.

There are at least two possible explanations for the discrepancy between fitted parameters and electrostatics for the three 6F-Trp analogs. According to our sensitivity analysis, the kinetic model is not very discriminating about the ion-binding affinity of the channel as long as the net translocation barrier height (the different central barrier height and well depth) is approximately correct. It is possible that small errors in the data lead to a normal affinity fit for the three 6F analogs. Alternatively, it is possible that the assumptions behind the Anderson et al. (2001) electrostatic profile are incorrect. For instance, a fluorine at indole position C6 would be more exposed to water than one at position C5. So, the charge distribution calculated in vacuum may be least appropriate for the 6F-analogs with modified Trps at positions 11, 13, and 15, closest to the bulk water. Additional work will be required to ascertain this profile correctly, taking environmental factors into account to better model the current data set as well as to correctly model the effect of Trp→Phe mutations for which the precise form of the profile is required.

In summary, we have collected a large set of single-channel current measurements in symmetrical KCl solutions for gA and each of eight fluorinated Trp analogs in each of two lipid bilayers. The data set sufficiently constrains the 3B2S kinetic model. The perturbations of the parameters are reasonably consistent with electrostatic predictions for five of the eight analogs, but for three of the 6F-analogs the 3B2S model requires increased binding affinity and translocation rate instead of the decreased affinity and modest effect on translocation rate predicted by electrostatics calculations. This discrepancy might be explored using heterodimer channels. If the electrostatic predictions are correct, gramicidin channels with the 6-F Trp at the exit only should exaggerate the exit rate effects, whereas those with the 5-F Trp at the entry only should exaggerate the trans-

location effects. Future work with such structural variants, more sophisticated permeation models, and electrostatic potentials are needed to resolve this discrepancy.

We are grateful to Joseph Gowen for some of the 6-F gA measurements reported here and to Mark Schumaker for helpful comments on the manuscript.

This project was supported by National Institutes of Health grant AI 23007.

REFERENCES

Andersen, O. S. 1983. Ion movement through gramicidin A channels: studies on the diffusion-controlled association step. *Biophys. J.* 41: 147–165.

Andersen, O. S., D. V. Greathouse, L. L. Providence, M. D. Becker, and R. E. Koeppe II. 1998. Importance of tryptophan dipoles for protein function: 5-fluorination of tryptophans in gramicidin A channels. *J. Am. Chem. Soc.* 120:5142–5146.

Anderson, D. G., R. B. Shirts, T. A. Cross, and D. D. Busath. 2001. Non-contact dipole effects on channel permeation. V. Computed potentials for fluorinated gramicidin. *Biophys. J.* 81:1255–1264.

Becker, M. D., D. V. Greathouse, R. E. Koeppe II, and O. S. Andersen. 1991. Amino acid sequence modulation of gramicidin channel function: effects of tryptophan-to-phenylalanine substitutions on the single-channel conductance and duration. *Biochemistry.* 30:8830–8839.

Busath, D. D., C. D. Thulin, R. W. Hendershot, L. R. Phillips, P. Maughan, C. D. Cole, N. C. Bingham, S. Morrison, L. C. Baird, R. J. Hendershot, M. Cotten, and T. A. Cross. 1998. Non-contact dipole effects on channel permeation. I. Experiments with (5F-indole)Trp-13 gramicidin A channels. *Biophys. J.* 75:2830–2844.

Cotten, M., C. Tian, D. Busath, R. Shirts, and T. A. Cross. 1999. Modulating dipoles for structure-function correlations in the gramicidin A channel. *Biochemistry.* 38:9185–9197.

Daumas, P., D. Benamar, F. Heitz, L. Ranjalahy-Rasoloarijao, R. Mouden, R. Lazaro, and A. Pullman. 1991. How can the aromatic side chains modulate the conductance of the gramicidin channel? A new approach using non-coded amino acids. *Int. J. Pept. Protein Res.* 38:218–228.

Daumas, P., F. Heitz, L. Ranjalahy-Rasoloarijao, and R. Lazaro. 1989. Gramicidin A analogs: influence of the substitution of the tryptophans by naphthylalanines. *Biochimie.* 71:77–81.

Doyle, D. A., J. M. Cabral, R. A. Pfuetzner, A. Kuo, J. M. Gulbis, S. L. Cohen, B. T. Chait, and R. MacKinnon. 1998. The structure of the potassium channel: molecular basis of K^+ conduction and selectivity. *Science.* 280:69–77.

Fields, C. G., G. B. Fields, R. L. Noble, and T. A. Cross. 1989. Solid phase peptide synthesis of ^{15}N-gramicidins A, B, and C and high performance liquid chromatographic purification. *Proc. Natl. Acad. Sci. U.S.A.* 85: 1384–1388.

Fonseca. V., P. Daumas, L. Ranjalahy-Rasoloarijao, F. Heitz, R. Lazaro, Y. Trudelle, and O. S. Andersen. 1992. Gramicidin channels that have no tryptophan residues. *Biochemistry.* 31:5340–5350.

Heinemann, S. H., H. Terlu, W. Stümher, K. Imoto, and S. Numa. 1992. Calcium channel characteristics conferred on the sodium channel by single mutations. *Nature.* 356:441–443.

Heitz, F., P. Daumas, N. Van Mau, R. Lazaro, Y. Trudelle, C. Etchebest, and A. Pullman. 1988. Linear gramicidins: influence of the nature of the aromatic side chains on the channel conductance. *In* Transport Through Membranes: Carriers, Channels, and Pumps. A. Pullman, J. Jortner, and B. Pullman, editors. Kluwer Academic Publishers, Dordrecht, The Netherlands. 147–165.

Heitz, F., C. Gavach, G. Spach, and Y. Trudelle. 1986. Analysis of the ion transfer through the channel of 9,11,13,15-phenylalanylgramicidin A. *Biophys. Chem.* 24:143–148.

Hall, J. E., C. A. Mead, and G. Szabo. 1973. A barrier model for current flow in lipid bilayer membranes. *J. Membr. Biol.* 11:75–97.

Hartmann, H. A., G. E. Kirsch, J. A. Drewe, M. Taglialatela, R. H. Joho, and A. M. Brown. 1991. Exchange of conduction pathways between two related K^+ channels. *Science.* 251:942–944.

Hille, B., and W. Schwarz. 1978. Potassium channels as multi-ion single-file pores. *J. Gen. Physiol.* 72:409–442.

Hinton, J. F., J. Q. Fernandez, D. C. Shungu, and F. S. Millet. 1988. Tl-205 NMR determination of the thermodynamic parameters for the binding of monovalent cations to gramicidins A and C. *Biophys. J.* 55:527–533.

Hladky, S. B. 1999. Can we use rate constants and state models to describe ion transport through gramicidin channels? *In* Proceedings of the Novartis Foundation Symposium 225: Gramicidin and Related Ion Channel-Forming Peptides. John Wiley and Sons, Chichester, UK. 93–111.

Hladky, S. B., and D. A. Haydon. 1984. Ion movements in gramicidin channels. *Curr. Top. Membr. Transp.* 21:327–372.

Imoto, K., C. Busch, B. Sakmann, M. Mishina, T. Konno, J. Nakai, H. Bujo, Y. Mori, K. Fukuda, and S. Numa. 1988. Rings of negatively charge amino acids determine the acetylcholine receptor channel conductance. *Nature.* 335:645–648.

Jan, L. Y., and Y. N. Jan. 1990. A superfamily of ion channels. *Nature.* 345:672.

Kim, K. S., D. P. Vercauteren, M. Welti, S. Chin, and E. Clementi. 1985. Interaction of K^+ ion with the solvated gramicidin A transmembrane channel. *Biophys. J.* 47:327–335.

Koeppe, R. E., J. L. Mazet, and O. S. Andersen. 1990. Distinction between dipolar and inductive effects in modulating the conductance of gramicidin channels. *Biochemistry.* 29:512–520.

MacKinnon, R., and G. Yellen. 1990. Mutations affecting TEA blockade and ion permeation in voltage-activated K^+ channels. *Science.* 250: 276–279.

McBride, D. W., Jr. 1981. Anomalous mole fraction behavior, momentary block, and lifetimes of gramicidin A in silver and potassium fluoride solutions. Ph.D. thesis. University of California, Los Angeles. 313 pp.

Pickar, A. D., and R. Benz. 1978. Transport of oppositely charged lipophilic probe ions in lipid bilayer membranes having various structures. *J. Membr. Biol.* 44:353–376.

Roux, B. 1999. Statistical mechanical equilibrium theory of selective ion channels. *Biophys. J.* 77:139–153.

Roux, B., and M. Karplus. 1993. Ion transport in the gramicidin channel: free energy of the solvated right-handed dimer in a model membrane. *J. Am. Chem. Soc.* 115:3250–3262.

Schumaker, M. F., R. Pomes, and B. Roux. 2001. Framework model for single proton conduction through gramicidin. *Biophys. J.* 80:12–30.

Thompson, N., G. Thompson, C. D. Cole, M. Cotten, T. A. Cross, and D. D. Busath. 2001. Non-contact dipole effects on channel permeation. IV. Kinetic model of 5F-Trp$_{13}$ gramicidin A currents. *Biophys. J.* 81: 1245–1254.

Urban, B., and S. B. Hladky. 1979. Ion transport in the simplest single file pore. *Biochim. Biophys. Acta.* 554:410–429.

Urban, B. W., S. B. Hladky, and D. A. Haydon. 1980. Ion movements in gramicidin pores: an example of single-file transport. *Biochim. Biophys. Acta.* 602:331–354.

Wang, K.-W., S. Tripathi, and S. B. Hladky. 1995. Ion binding constants for gramicidin A obtained from water permeability measurements. *J. Membr. Biol.* 143:247–257.

Williamson, A. V., and W. A. Sather. 1999. Nonglutamate pore residues in ion selection and conduction in voltage-gated Ca^{2+} channels. *Biophys. J.* 77:2575–2589.

Yang, J., P. T. Ellinor, W. A. Sather, J. F. Zhang, and R. W. Tien. 1993. Molecular determinants of Ca^{2+} selectivity and ion permeation in L-type Ca^{2+} channels. *Nature.* 366:158–161.

Yool, A. J., and T. L. Schwarz. 1991. Alteration of ionic selectively of a K^+ channel by mutation of the H5 region. *Nature.* 349:700–704.